

## Supporting Information

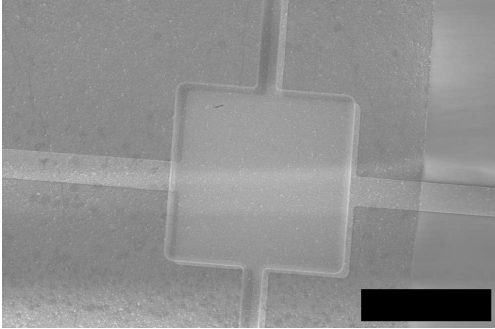
### Supporting Information Outline:

1. Devices Studied and Characterization
2. Fabrication
3. Derivation of the Photon-Induced Rigidity
4. Estimating Photon-Induced Rigidity
5. Photon-Induced Rigidity:  $\lambda$  and  $V_g$  Dependence
6. Radiation Pressure Effects
7. Fitting to Frequency versus Gate Voltage
8. Injection Locking Behavior
9. Derivation of Reflectivity and Absorption
10. Minimum  $T$  from Photothermal Cooling

### 1. Devices Studied and Characterization

We primarily studied two devices for this article, which we call “Device 1” and “Device 2.” SEM images for both are displayed in Fig. S1.

#### Device 1



#### Device 2

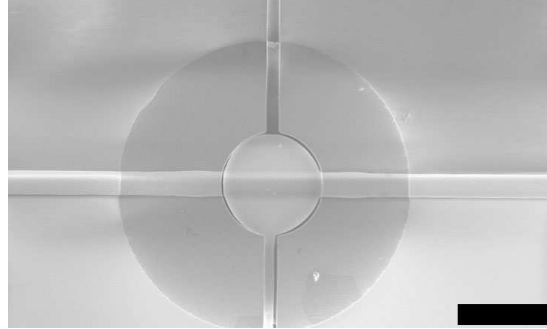


**Fig. S1.** Device 1 (left) and Device 2 (right). Scale bars are  $10\mu\text{m}$ . Graphene is suspended over a square (Device 1) or circular (Device 2) trench in  $\text{SiO}_2$ . An additional trench extends vertically from the top and bottom of each square/circular trench to allow liquid to drain from beneath the graphene after transfer. Platinum source and drain electrodes contact the graphene from the underside. A gate electrode lies along the bottom of each trench.

Device properties are listed in Table S1. The density  $\rho$  and initial tension  $\sigma_0$  are determined by fitting frequency as a function of gate voltage, as described in Section 7. All other data are measured experimentally. We measure the distance  $d$  between the graphene and the electrode in the absence of a gate voltage using an optical profilometer. We measure the length  $L$  along the side of Device 1 and the radius  $a$  of Device 2 from SEMs.

**Table S1. Graphene device properties**

Device	Dimension ( $\mu\text{m}$ )	$d$ ( $\mu\text{m}$ )	$\rho / \rho_{\text{graphene}}$	$\sigma_0$ (N/m)
1	$L/2 = 7.0 \pm 0.1$	1.96	$4.6 \pm 0.3$	$0.013 \pm 0.001$
2	$a = 5.5 \pm 0.1$	1.37	$2.9 \pm 0.2$	$0.010 \pm 0.001$

## 2. Fabrication

The procedure for fabricating devices was based on an earlier article (1). Fabrication began with the thermal growth of 240 nm SiO<sub>2</sub> on a 10 kΩ·cm Si wafer. Trenches were patterned in the SiO<sub>2</sub> / Si using photolithography followed by reactive ion etching. Etching of the trenches consisted of two steps: first, a directional CHF<sub>3</sub> / O<sub>2</sub> or CF<sub>4</sub> etch was used to etch the SiO<sub>2</sub> and Si; then, an isotropic SF<sub>6</sub> / O<sub>2</sub> etch was used to create an undercut profile in the Si beneath the oxide (~200 nm undercut). The undercut was designed to prevent shorting between the source/drain and gate electrodes during the following metal evaporation step. After the etch, an additional 220 nm of oxide was thermally grown. Next, source, drain, and gate electrodes were patterned in a single photolithography step, followed by e-beam evaporation of 5 nm Ti / 25 nm Pt.

Graphene was grown by CVD on copper foil and transferred using the method developed by Li et al. (2). To make Device 1, graphene on Cu foil was patterned into 50 μm x 50 μm squares using photoresist and contact lithography followed by O<sub>2</sub> plasma etching (1). The resist was removed by sonication in Microposit Remover 1165 (n-methyl-pyrrolidinone), and 4% 495k MW poly(methyl methacrylate) (PMMA) in anisole was spun onto the surface of the graphene/copper. The copper was etched in ferric chloride; the graphene was rinsed by transferring it to several water baths and finally transferred to the substrate. The squares of graphene landed randomly in this procedure. The PMMA was removed in dichloromethane, and the devices were rinsed in IPA and critical point dried to prevent stiction.

Device 2 was patterned via a novel procedure designed to improve yield. Graphene grown on Cu foil was transferred directly to the substrate using PMMA as the support layer as described above. Importantly, however, after spinning PMMA onto the graphene on Cu foil, the foil was baked on a hotplate at 170°C for 5 minutes. After transfer, a layer of Shipley 1813 resist was spun on top of the PMMA and the resist was patterned using optical lithography. Then, oxygen plasma was used to etch the pattern into the PMMA and graphene. Finally, the resist and PMMA were both removed using Microposit Remover 1165. The chip was transferred to IPA and critical point dried.

## 3. Derivation of the Photon-Induced Rigidity

According to (3), the effective frequency  $\omega_{eff}$  and damping  $\Gamma_{eff}$  should follow:

$$\omega_{eff}^2 = \omega_0^2 \left( 1 - \frac{1}{1 + \omega_0^2 \tau^2} \frac{\nabla F}{K} \right) \quad (\text{S-1})$$

$$\Gamma_{eff} = \Gamma \left( 1 + Q \frac{\omega_0 \tau}{1 + \omega_0^2 \tau^2} \frac{\nabla F}{K} \right) \quad (\text{S-2})$$

Here, we derive  $\nabla F_{pth} \equiv dF_{pth} / dz$  for our optomechanical system, where  $F_{pth}$  is the photothermal force felt by the membrane. We use the model illustrated in Fig. S-2, in which a fully clamped circular graphene membrane with radius  $a$  and initial tension per unit length along the perimeter  $\sigma_0$  is suspended a distance  $d$  away from a gate electrode. Let  $z$  denote the vertical displacement of the center of the graphene membrane, and  $z_0$  its

equilibrium displacement from the flat membrane case due to an applied gate voltage. Our goal is to find the photothermal spring constant for small oscillations about  $z = z_0$ .

We start by assuming that heating from the laser causes a tension change in the graphene proportional to the power of the electric field at position  $z$ :

$$\sigma_{pth} = AP \sin^2 \left( \frac{2\pi}{\lambda} (d - z) \right) \quad (\text{S-3})$$

where  $P$  is the incident laser power and  $\lambda$  is the laser wavelength. Assuming the tension arises from laser-induced heating, the proportionality constant  $A$  depends on many theoretical factors such as graphene's light absorption, thermal conductivity, and thermal expansion coefficient, but it can also be determined empirically (see Section 4).

The external force that the contact exerts on the membrane is given by the  $z$ -component of the tension induced by the laser:  $F_{cont} = -2\pi a \sigma_{pth} \sin \theta$ , where  $\theta$  is the contact angle (a function of  $z$  and gate voltage). The gradient is then

$$\nabla F_{cont} = -2\pi a \left[ \sin \theta \nabla \sigma_{pth} + \sigma_{pth} \nabla \sin \theta \right]_{z=z_0}$$

The first term is  $\nabla F_{pth}$  and has a time constant  $\tau_{pth}$  associated with it, which depends on the thermal conductivity and specific heat capacity of graphene. The second term is related to the change in the contact angle as the membrane moves, which happens instantaneously and serves only to offset the mechanical spring constant  $K$ .

Thus, the photothermal spring constant is given by

$$\nabla F_{pth} = AP \frac{4\pi^2 a}{\lambda} \sin \theta_0 \sin \left( \frac{4\pi}{\lambda} (d - z_0) \right) \quad (\text{S-4})$$

where  $\theta_0 = \theta(z_0)$ . Note that  $\nabla F_{pth} = 0$  when  $\theta_0 = 0$ , meaning that the membrane must start with a nonzero displacement in order to experience optomechanical effects. In other words, a gate voltage must be applied to the membrane to break the symmetry; if the membrane were perfectly flat, the tension change due to the laser would act perpendicular to the degree of freedom and would not affect the motion. For the optomechanical system described in Ref. 4, this asymmetry condition is satisfied by making the resonator from two different materials to act as a bimetallic strip.

Next, we find the equilibrium position of the membrane as a function of gate voltage. Assume that the shape of the membrane forms a spherical cap as it is pulled down by the electrostatic force from the gate (5). The position of the center of the membrane is related to the contact angle by

$$z_0 = a \frac{1 - \cos \theta_0}{\sin \theta_0} \quad (\text{S-5})$$

The net external force on the membrane must be zero, so the upward force of the contact is equal to the downward force of the gate voltage. The total stress is

$\sigma_{tot} = \sigma_0 + \frac{E}{1-\nu} \frac{\Delta L}{L} + \sigma_{pth}$ , where  $\sigma_0$  is the initial tension in the device in the absence of a gate voltage or laser,  $E$  is the 2D Young's modulus (in N/m),  $\nu$  is the Poisson ratio, and the strain  $\frac{\Delta L}{L} = \frac{\theta_0}{\sin \theta_0} - 1$ . The electrostatic force is given by  $F_{gate} = \frac{1}{2} \frac{dC}{dz} V_g^2$ , where  $C$  is the capacitance of the device. Assuming the membrane and the gate electrode form the

two sides of a parallel plate capacitor,  $\frac{dC}{dz} = \frac{\epsilon_0 \pi a^2}{(d - z_0)^2}$ . We arrive at an equation for the equilibrium position of the membrane:

$$\frac{E}{1-\nu} \theta_0 - \sin \theta_0 \left( \frac{E}{1-\nu} - \sigma_0 - AP \sin^2 \left( \frac{2\pi}{\lambda} (d - z_0) \right) \right) = \frac{\epsilon_0 a V_g^2}{4(d - z_0)^2} \quad (\text{S-6})$$

where  $z_0$  is given by Eq. S-5.

Expanding this equation to first order in  $\theta_0$  gives

$$\theta_0 = \frac{\epsilon_0 a d V_g^2}{4d^3 (\sigma_0 + AP \sin^2(2\pi d / \lambda)) - \epsilon_0 a^2 V_g^2} \quad (\text{S-7})$$

We can solve Eq. S-6 numerically by using specific parameters from one of our devices, and we find that the first order approximation of  $\theta_0$  departs from the exact value quickly, at around  $V_g = 5$  V for Device 2.

Note that when  $V_g$  is small,  $\nabla F_{pth} \propto P V_g^2$  (see Fig. S-5). Hence, the observed optomechanical effects depend strongly on gate voltage. In addition, by using the gate voltage to pull the graphene membrane through a node in the optical field, we can cause  $\nabla F_{pth}$  to change sign, thereby enhancing or reducing the damping.

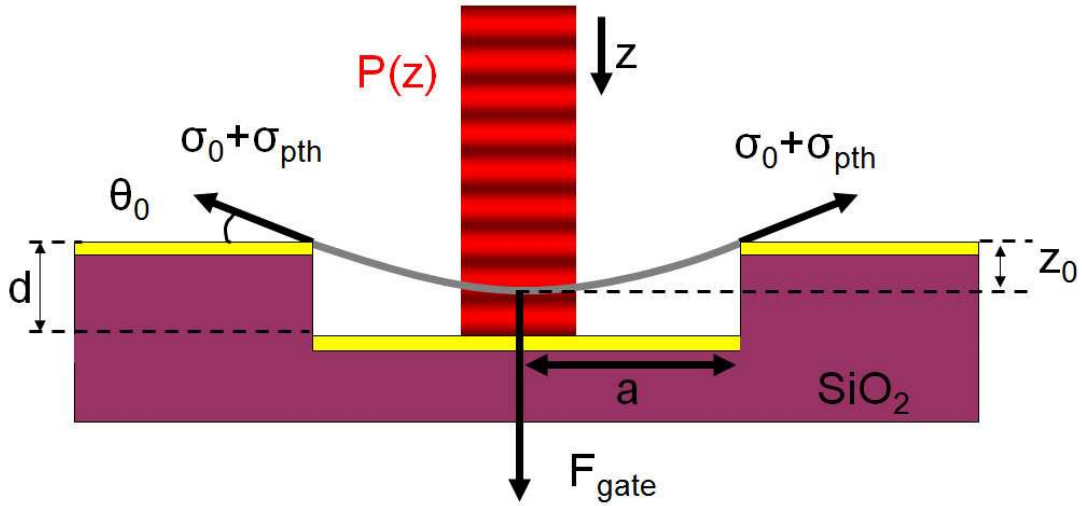


**Fig. S-2.** Schematic of the model used to estimate the size of the photothermal effect. The color of the incident light beam represents the energy density in the electric field, which is proportional to the absorbed energy flux  $W_a(z)$ . The photothermal spring constant is proportional to the gradient of the field.

#### 4. Estimating Photon-Induced Rigidity

##### Determining the Constant A Experimentally

We use the frequency of the graphene as a function of laser power at low gate voltage to obtain an experimental measure of  $A$  for Device 2. The frequency of a circular drumhead resonator is given by:

$$f = \frac{2.404}{2\pi a} \sqrt{\frac{\sigma}{\rho}}$$

where we assume  $\sigma = \sigma_0 + \sigma_{\text{pth}}$  is the stress in the resonator in the absence of gate voltage. In the limit of  $\sigma_{\text{pth}} \ll \sigma_0$ , we can expand this to find:

$$f \approx \frac{2.404}{2\pi a} \sqrt{\frac{\sigma_0}{\rho}} \left( 1 + \frac{\sigma_{\text{pth}}}{2\sigma_0} \right) \quad (\text{S-8})$$

In order to get an estimate for  $A$ , we measure the frequency versus laser power at a gate voltage ( $V_g = 0.8$  V) that is too low to significantly affect the tension or cavity length, but high enough to make the device resonate at a detectable amplitude (Fig. S-3). Fitting Eq.

S-8 and Eq. S-3 to the data in Fig. S-3 yields  $f_0 \equiv \frac{2.404}{2\pi a} \sqrt{\frac{\sigma_0}{\rho}} = 5.042 \pm .005$  MHz and  $A = 15$  N/(m·W) using the values from Table S-1.

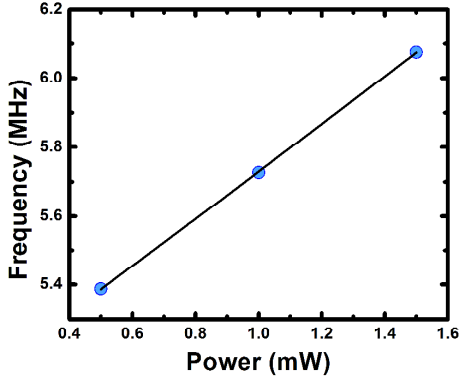


**Fig. S-3.** Frequency of Device 2 at  $V_g = 0.8$  V as a function of laser power.

We can also estimate  $A$  from thermal expansion. Assuming pure thermal expansion in a circular membrane and absorption  $\pi\alpha$  (see Section 9), we find that in the cavity  $A = -2 \alpha E \alpha_g / t \kappa (1 - \nu) = 4$  N/m·W, where  $\alpha$  is the fine structure constant,  $\kappa = 5000$  W/m·K is the thermal conductivity (6),  $E \approx 60$  N/m is the Young's modulus of CVD graphene (7),  $t = 0.335$  nm is the thickness of graphene,  $\alpha_g \approx -7 \times 10^{-6}$  is the thermal expansion coefficient of graphene (8), and  $\nu = 0.16$  is the Poisson ratio for graphene. This value is in reasonable agreement with the experimentally determined value of  $A = 15$  N/m·W considering the assumptions and the uncertainty in the theoretical numbers, especially Young's modulus (7).

### Estimating $\tau$

In order to compare the size of the observed optomechanical effect to that predicted by Eq. S-2 and S-4, we must estimate  $\tau$ . Assuming a circular membrane resonator, the thermal equilibration time constant can be approximated as  $\tau = a^2 \rho C / 2\kappa$ , where  $C = 700$  J/(kg·K) is the specific heat of the graphene and  $\kappa = 5000$  W/(m·K) is the thermal conductivity. For the circular membrane resonator observed here,  $\tau = 5$  ns.

### Estimating Photon-Induced Rigidity

We can compare these values to the experimentally obtained values for Device 2 in Fig. 3c-d. The slope of Fig. 3d together with Eq. S-2 yields an experimental value of  $\frac{d\nabla F}{dP} = 0.7 \text{ N}/(\text{m}\cdot\text{W})$ . The value predicted by Eq. S-4, using Eq. S-7 to find  $\theta_0$ , is  $\frac{d\nabla F}{dP} = 4.4 \text{ N}/(\text{m}\cdot\text{W})$ . For Fig. 3c, the experimental number is  $\frac{d\nabla F}{dP} = -17 \text{ N}/(\text{m}\cdot\text{W})$ , while the theoretical estimate is  $\frac{d\nabla F}{dP} = -202 \text{ N}/(\text{m}\cdot\text{W})$ , where this time Eq. S-6 must be solved to find  $\theta_0$ . This agreement is reasonable considering the important dependence on  $\theta_0$  and  $z_0$ , which must be estimated theoretically, and the approximations involved in our model (we ignore the curvature of the membrane in the light field and the finite laser spot size).

## 5. Photon-Induced Rigidity: $\lambda$ and $V_g$ Dependence

### Dependence on Wavelength $\lambda$

The above theory for photothermal optomechanical coupling makes several predictions that can be tested experimentally. First, the optomechanical damping  $\Gamma_{\text{OM}}$  should depend sinusoidally on laser wavelength. We use a tunable-wavelength Ti:Sapphire laser to test this hypothesis on Device 2 from  $\lambda = 700\text{nm}$  to  $\lambda = 840 \text{ nm}$ . Figure S-4 shows that the theory (Eq. S-2 and S-4) predicts the damping accurately over this range. To fit the frequency, we use a modified version of Eq. S-1 that takes into account both static absorption-induced stress and optomechanical back-action:

$$\omega_{\text{eff}}^2 = \omega_0^2 \left( 1 + B \sin^2 \left( \frac{2\pi}{\lambda} (d - z) \right) - \frac{C}{\lambda} \sin \left( \frac{4\pi}{\lambda} (d - z) \right) \right) \quad (\text{S-1a})$$

where  $B$  and  $C$  are proportionality constants. This modified version captures the trend in the data. We note that according to theory,  $B = A P / \sigma$  (Eqs. S-3 and S-8), and  $C = 4\pi^2 a A P \sin\theta_0 \text{ K}^{-1} (1 + \omega_0^2 \tau^2)^{-1}$  (Eq. S-4). If we leave  $B$ ,  $C$ , and  $\omega_0$  as fit parameters, we find  $B = 1.13$ ,  $C = 400 \text{ nm}$ , and  $\omega_0 = 12 \text{ MHz}$ . These numbers agree well with the theoretical values of  $B = 0.71$  and  $C = 800 \text{ nm}$ , where we have used  $\sigma = (\omega_0/2.404)^2 a^2 \rho = 0.064 \text{ N}/\text{m}$  to find  $B$  theoretically.

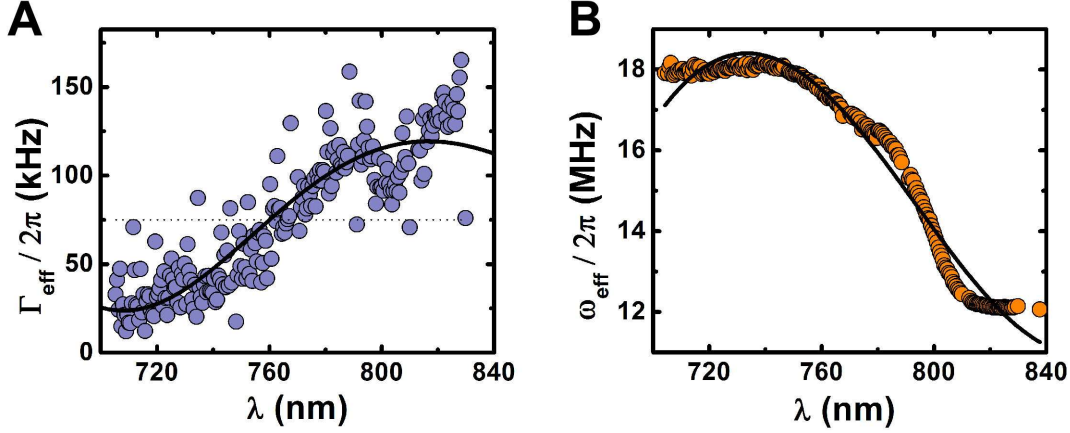


**Fig S-4.** (A) Damping of Device 2 at  $V_g = 16$  V,  $P = 3$  mW as a function of wavelength. The dotted line indicates the intrinsic damping measured at low laser power. The black line is a fit to Eq. S-2 with  $d-z = 1330$  nm (measured at  $V_g = 16$  V from where  $dR(\lambda)/dz = 0$ ). (B) Frequency as a function of wavelength for the same measurement. The black line is a fit to Eq. S-1a with  $d-z = 1330$  nm.

Equation S-4 also predicts a dependence of the optomechanical damping on gate voltage, since  $\theta_0$  is a function of  $V_g$ . For small  $V_g$  and  $P$ , we find that  $\theta_0 \propto V_g^2$ , and therefore  $\Gamma_{OM} \propto PV_g^2$ . Figure S-5 shows the measured optomechanically-induced damping as a function of  $V_g^2$  for two different laser powers, which agrees well with this prediction.

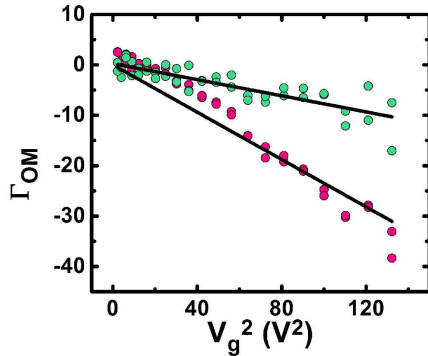


**Fig S-5.** Optomechanically induced damping  $\Gamma_{OM}$  for Device 1 at a given laser power (shown for 0.3 mW, green; and 2 mW, pink) depends on gate voltage roughly as  $V_g^2$ . We determine  $\Gamma_{OM} = \Gamma_{\text{eff}} - \Gamma$  by assuming the intrinsic damping  $\Gamma$  can be measured at low laser power. We use  $\Gamma = \Gamma_{\text{eff}} (P = 100 \mu\text{W})$ . Black lines are linear fits to the data with a y-intercept of  $\Gamma_{OM}(V_g = 0) = 0$ .

## 6. Radiation Pressure Effects

We also consider the possibility of an optomechanical effect from radiation pressure. According to Ref. 3, the maximal force gradient due to radiation pressure is:

$$\nabla F_{rad} = \frac{2P}{c\lambda} 2\sqrt{R_g} g^2 \quad (\text{S-9})$$

where  $g^2 = 4R/(1-R)^2$  is the coefficient of finesse,  $R = (R_g R_e)^{1/2}$ ,  $R_g$  is the reflectance of the graphene, and  $R_e \approx 1$  is the reflectance of the platinum electrode. Using  $R_g \approx \pi^2 \alpha^2 (1 - \pi\alpha)/4 = 1.3 \times 10^{-4}$  (see Section 9), at  $P = 5$  mW and  $\lambda = 633$  nm, we find  $\nabla F_{rad} \approx 5 \times 10^{-7}$  N/m, which is too small compared to the resonator spring constant  $K = 0.1$  N/m to be of significance.

## 7. Fitting to Frequency versus Gate Voltage

We are able to infer the mass and initial tension of the resonators by fitting a tensioned membrane model to the frequency versus gate voltage data, taken at low laser power such that optomechanical effects are negligible. We apply the theory in Ref. 5 to a fully clamped 2D membrane in the shape of a spherical cap. Let  $S$  be the radius of curvature of the spherical cap. Equating the force from the contact to the electrostatic

force from the gate gives the total tension:  $\sigma = \frac{S}{2\pi a^2} F_{gate}$ . The additional tension

induced by stretching is  $\sigma - \sigma_0 = \frac{E}{1-\nu} \frac{\Delta L}{L} \approx \frac{E}{1-\nu} \frac{a^2}{6S^2}$ , assuming the strain  $\Delta L/L$  is small.

Combining these equations to eliminate  $S$  gives a cubic equation for the tension:

$$\sigma^2(\sigma - \sigma_0) = \frac{E}{1-\nu} \frac{F_{gate}^2}{24\pi^2 a^2} \quad (\text{S-10})$$

The frequency of a tensioned circular resonator is given by  $f = \frac{2.404}{2\pi a} \sqrt{\frac{\sigma}{\rho}}$ , where  $\rho$  is the

2D mass density. Assume the electrostatic force is that of a parallel plate capacitor:  $F_{gate} = \varepsilon_0 \pi a^2 V_g^2 / 2d^2$ . Note that in the limit of low tension ( $\sigma \approx \sigma_0$ ), Eq. S-10 suggests that  $f$  scales as  $V_g^2$ , while in the limit of high tension ( $\sigma \gg \sigma_0$ ) it scales as  $V_g^{2/3}$ .

We fit the following model to our frequency versus gate voltage data, using a nonlinear least squares method:

$$\left(f^2 - c_3 V_g^2 - c_1\right) \left(f^2 - c_3 V_g^2\right)^2 = c_2 V_g^4 \quad (\text{S-11})$$

where  $c_1$ ,  $c_2$ , and  $c_3$  are fitting parameters. In terms of the theory outlined above,

$$c_1 = \frac{2.404^2}{4\pi^2 a^2} \frac{\sigma_0}{\rho} \quad \text{and} \quad c_2 = \frac{2.404^6 \varepsilon_0^2}{6144\pi^6 a^4 d^4 \rho^3} \frac{E}{1-\nu}. \quad \text{Hence, we can extract initial tension } \sigma_0$$

and density  $\rho$  from these two parameters. We add in the parameter  $c_3$  to represent an offset to the spring constant proportional to  $V_g^2$ , which matches our data at low gate voltages. This term can arise from capacitive softening (9), however, if we use the density derived from  $c_2$ , we predict that  $c_3$  should be much larger than what we observe. We suspect that there are other physical mechanisms that determine  $c_3$ , such as regions of initial slack (10).

The data and fits for our two devices are plotted in Fig. S-6. The model fits well at low gate voltage and gives us reasonable values for  $\sigma_0$  and  $\rho$ , but at high gate voltage the

frequency continues to increase when the model's  $V_g^{2/3}$  dependence rolls off. This is the subject of ongoing research.

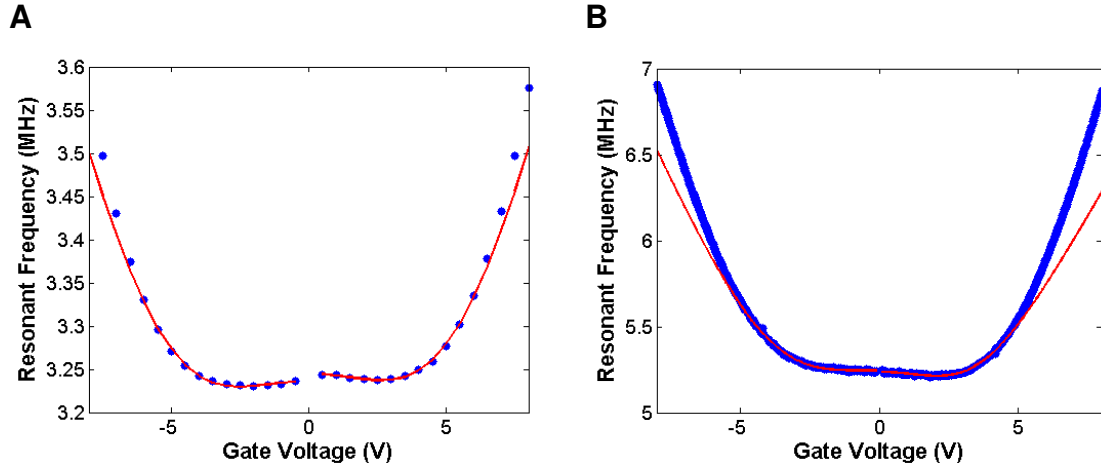


**Fig. S-6.** Frequency versus gate voltage for Device 1 (A) and Device 2 (B). The blue dots are the data and the red lines are the fits. We only fit to  $V_g^2 < 40 \text{ V}^2$  for Device 1, and  $V_g^2 < 20 \text{ V}^2$  for Device 2. At higher gate voltages the tensioned membrane model diverges from the data.

## 8. Injection Locking Behavior

When the graphene is self-oscillating and a small electrical drive signal is applied, the graphene membrane motion locks to the drive signal (Fig. S-7). The jump in frequency near  $V_g = 5 \text{ V}$  appears only at high laser power and is likely related to previously observed interactions between the photothermal force and the electrical force governing the length of the cavity (11).

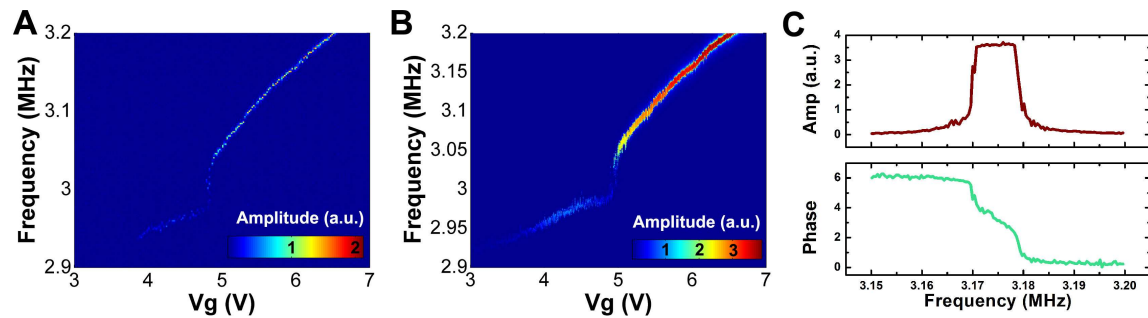


**Fig. S-7.** Injection locking behavior in Device 1. (A) No drive; the self-oscillation frequency of the device tunes with gate voltage. (B) An electrical driving force (-60 dBm) is applied between the gate and the drain. (C) Amplitude and phase versus frequency at  $V_g = 6.17 \text{ V}$  from the data in (B).

We also observe injection locking to a modulated optical signal, with no modulated voltage applied to the graphene (Fig. S-8).

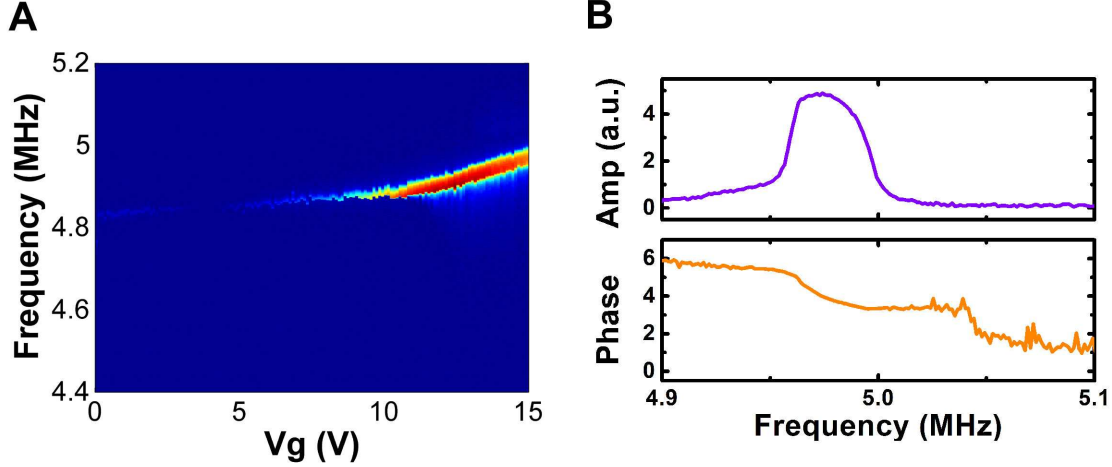


**Fig. S-8.** Locking to an optical signal in Device 1. (A) An optically modulated signal ( $\lambda = 405$  nm,  $P = 1.8$  mW) is used to drive the graphene motion; a red laser ( $\lambda = 633$  nm,  $P = 2$  mW) is used to read the motion. The reflected light is filtered so that only the  $\lambda = 633$  nm light is detected by the photodiode. For  $V_g > 10$  V, the graphene exhibits self-oscillation and locks to the drive signal. (B) Amplitude and phase versus frequency at  $V_g = 15$  V from the data in (A).

## 9. Derivation of Reflectivity and Absorption

### Cavity Reflectivity

The amplitude and phase of the reflected light is what we measure experimentally using a photodiode and network analyzer, in order to determine the graphene resonator's amplitude of motion. Here we calculate the overall cavity reflectivity in terms of the electric field of the incident and reflected plane waves,  $R = \left| \vec{E}_{reflected} \right|^2 / \left| \vec{E}_{incident} \right|^2$ , as a function of position of the graphene membrane. We start by assuming the graphene is an infinitely thin conducting sheet with a reflection coefficient  $r_g$ , a transmission coefficient  $t_g$ , and a distance  $d$  away from a perfectly conducting back plane (the platinum gate electrode). Summing over contributions from every reflected wave, the reflection coefficient of the cavity is given by

$$r = - \left( r_g + \frac{t_g^2 e^{i\phi}}{1 - r_g e^{i\phi}} \right),$$

where  $\phi = 4 \pi d / \lambda$  is the phase difference obtained from one round trip inside the cavity. The minus sign accounts for the  $\pi$  phase shift due to reflection off a conducting surface; each wave contributing to the sum reflects an odd number of times. The cavity reflectivity is then given by the magnitude of the reflection coefficient squared:

$$R = |r|^2 = r_g^2 - t_g^2 + \frac{t_g^2 (1 - r_g^2 + t_g^2)}{1 + r_g^2 - 2r_g \cos \phi} \quad (\text{S-12})$$

The transmittance and reflectance of graphene can be derived by applying Maxwell's equations and the appropriate boundary conditions at the graphene, while assuming the conductivity is small (12,13):  $T_g = (1 + \pi\alpha/2)^{-2}$ ,  $R_g = (\pi\alpha)^2 T/4$ , where  $\alpha =$

1/137 is the fine structure constant. The reflection and transmission coefficients are then found by taking the square root:

$$r_g = \frac{\pi\alpha}{2 + \pi\alpha} \quad t_g = \frac{2}{2 + \pi\alpha}$$

Plugging these into Eq. S-12 gives the cavity reflectivity as a function of cavity detuning, which we have plotted in Fig. 2c.

### Graphene Absorbed Energy

The amount of energy the graphene absorbs from the spatially varying electric field can be calculated from the interaction between light and Dirac fermions, and is proportional to the magnitude of the electric field squared:  $W_a = \pi\alpha c\epsilon_0|E|^2$ , where  $c$  is the speed of light, and  $\epsilon_0$  is the permittivity of free space (12). Because the reflection coefficient of graphene is small ( $r_g \sim 0.01$ ), we can assume that the total electric field is mostly determined by the sum of a single incident plane wave moving toward the back plane, and a single reflected plane wave moving away from it. The result is  $|E|^2 = 4|E_0|^2 \sin^2(2\pi d/\lambda)$ , where  $E_0$  is the complex amplitude of the incoming plane wave. The factor of 4 comes from the fact that the incident and reflected waves combine constructively, doubling the amplitude of the electric field. We normalize  $W_a$  by the energy flux of the incident plane wave,  $W_i = c\epsilon_0|E_0|^2$ , to get the absorption as a function of position:

$$W_a / W_i = 4\pi\alpha \sin^2(2\pi d / \lambda) \quad (\text{S-13})$$

Equation S-13 is also plotted in Fig. 2c.

## 10. Minimum $T$ from Photothermal Cooling

We include a brief discussion of the prospects for photothermal cooling of membrane resonators to the quantum ground state. First, we note that the effective temperature  $T_{\text{eff}}$  reached using laser cooling from a bath temperature  $T$  is given by (3):

$$\frac{T_{\text{eff}}}{T} = \frac{1}{1 + Q_M \frac{\omega_0 \tau}{1 + \omega^2 \tau^2} \frac{\nabla F}{K}} \quad (\text{S-14})$$

We assume the optimal cooling condition  $\omega_0 \tau = 1$ . The photon-induced rigidity for arbitrary cavity detuning  $\varphi_0 = \frac{4\pi}{\lambda}(d - z_0)$  is  $\nabla F = \eta \sin(\varphi_0)P$ , where

$\eta = (4\pi^2 a / \lambda)A \sin \theta_0$  denotes the linear power dependence of  $\nabla F$ . In this work, we measured  $\eta \sin \varphi_0 = -17 \text{ N}/(\text{m}\cdot\text{W})$  for Device 2 at  $V_g = -10\text{V}$ . To obtain a conservative estimate, we assume that this value corresponds to the maximal optomechanical force gradient, i.e.  $\eta = 17 \text{ N}/(\text{m}\cdot\text{W})$ . Thus we have:

$$\frac{T}{T_{\text{eff}}} = \frac{\Gamma_{\text{eff}}}{\Gamma} = 1 + \frac{Q_M}{2} \frac{\eta \sin \varphi_0}{K} P \quad (\text{S-15})$$

The minimum  $T_{\text{eff}}$  is limited by the fact that the laser heats the entire membrane as it is cooling a single mechanical mode. To account for this effect, when the laser causes a temperature rise  $\Delta T$ , we must replace the bath temperature  $T$  with  $T + \Delta T$ . Following

Ref. 3, the absorbed laser power  $P_a$  causes a temperature rise  $\Delta T = \beta P_a$ , where  $\beta$  is a proportionality constant given by  $\beta = (2 \pi t \kappa)^{-1}$ . From Eq. S-13,  $P_a = 4\pi\alpha \sin^2(2\pi d/\lambda) P$ . Thus we have

$$\frac{T + \Delta T}{T_{eff}} = \frac{T + 4\pi\alpha\beta \sin^2(\varphi_0/2)P}{T_{eff}} = \frac{\Gamma_{eff}}{\Gamma}$$

$$T_{eff} = \left( T + 4\pi\alpha\beta \sin^2(\varphi_0/2)P \right) \left/ \left( 1 + \frac{Q_M}{2} \frac{\eta \sin \varphi_0}{K} P \right) \right. \quad (\text{S-16})$$

As an example, we will use the resonator from (1), which had  $\omega_0 = 2\pi \times 75$  MHz and  $Q = 9000$  at a temperature of  $T = 9$  K. Taking a typical  $K = 0.1$  N/m and a detuning of  $\varphi_0 = \pi/10$ ,  $P = 15$  mW leads to an effective temperature  $T_{eff} = 3.4$  mK, comparable to the ground state temperature of  $T_Q = 3.6$  mK while satisfying the stability condition  $\nabla F / K < 1$ .

Note that S-16 favors detuning the cavity toward the point of minimal absorption, which increases the size of the optomechanical effect relative to the amount of absorbed laser power. The ability to detune the cavity with gate voltage is a crucial advantage in this respect.

### Supporting References

- <sup>1</sup> A. M. van der Zande et al., Large-Scale Arrays of Single-Layer Graphene Resonators. *Nano Letters* **10**, 4869 (2010).
- <sup>2</sup> X. S. Li et al., Large-Area Synthesis of High-Quality and Uniform Graphene Films on Copper Foils. *Science* **324**, 1312 (2009).
- <sup>3</sup> C. Metzger, I. Favero, A. Ortlieb, K. Karrai, Optical self cooling of a deformable Fabry-Perot cavity in the classical limit. *Physical Review B* **78**, 035309 (2008).
- <sup>4</sup> C. H. Metzger, K. Karrai, Cavity cooling of a microlever. *Nature* **432**, 1002 (2004).
- <sup>5</sup> C. Y. Chen et al., Performance of monolayer graphene nanomechanical resonators with electrical readout. *Nature Nanotechnology* **4**, 861 (2009).
- <sup>6</sup> A. A. Balandin et al., Superior thermal conductivity of single-layer graphene. *Nano Letters* **8**, 902 (2008).
- <sup>7</sup> C. S. Ruiz-Vargas et al., Softened Elastic Response and Unzipping in Chemical Vapor Deposition Graphene Membranes. *Nano Letters* **11**, 2259 (2011).
- <sup>8</sup> W. Z. Bao et al., Controlled ripple texturing of suspended graphene and ultrathin graphite membranes. *Nature Nanotechnology* **4**, 562 (2009).

- <sup>9</sup> V. Singh et al., Probing thermal expansion of graphene and modal dispersion at low-temperature using graphene nanoelectromechanical systems resonators. *Nanotechnology* **21**, 165204 (2010).
- <sup>10</sup> V. Sazonova *et al.*, A tunable carbon nanotube electromechanical oscillator. *Nature* **431**, 284 (2004).
- <sup>11</sup> M. Vogel, C. Mooser, K. Karrai, R. J. Warburton, Optically tunable mechanics of microlevers. *Applied Physics Letters* **83**, 1337 (2003).
- <sup>12</sup> R. R. Nair *et al.*, Fine structure constant defines visual transparency of graphene. *Science* **320**, 1308 (2008).
- <sup>13</sup> L.A. Falkovsky, Optical properties of graphene. *Journal of Physics: Conference Series* **129**, 012004 (2003).

